Audio Engineering Society

Convention Paper

Presented at the 139th Convention
2015 October 29–November 1 New York, USA

An Improved and Generalized Diode Clipper Model for Wave Digital Filters

Kurt James Werner[1], Vaibhav Nangia[1], Alberto Bernardini[2], Julius O. Smith III[1], Augusto Sarti[2]

[1] *Center for Computer Research in Music and Acoustics (CCRMA), Stanford University, Stanford, CA 94305, USA*

[2] *Dipartimento di Elettronica, Informazione e Bioingegeria, Politecnico di Milano, 20133 Milan, Italy*

Correspondence should be addressed to Kurt James Werner (`kwerner@ccrma.stanford.edu`)

ABSTRACT

We derive a novel explicit wave-domain model for "diode clipper" circuits with an arbitrary number of diodes in each orientation, applicable, e.g., to wave digital filter emulation of guitar distortion pedals. Improving upon and generalizing the model of Paiva *et al.* (2012), which approximates reverse-biased diodes as open circuits, we derive a model with an approximated correction term using two Lambert $\mathcal{W}$ functions. We study the energetic properties of each model and clarify aspects of the original derivation. We demonstrate the model's validity by comparing a modded Tube Screamer clipping stage emulation to SPICE simulation.

1. INTRODUCTION

The field of Virtual Analog (VA) is concerned with creating digital imitations of analog musical devices. A popular approach to VA called physical modeling [1] involves discretizing continuous-time descriptions of a system's physics. In physical modeling, the Wave Digital Filter (WDF) concept [2] has been used extensively. In "Emulation of Operational Amplifiers and Diodes in Audio Distortion Circuit," Paiva *et al.* used the Lambert $\mathcal{W}$ function to create a simplified, explicit, wave-domain model of "diode clippers," which are of particular interest for modeling guitar distortion pedals and effects [3].

In this paper, we propose novel improvements to and generalizations of the work of Paiva *et al.*, yielding explicit wave-domain models for generalized diode clippers with significantly reduced approximation error. In §2, previous work on WDF models of diode clippers is reviewed, especially the Paiva *et al.* model [3]. Novel alternative (§3) and improved models (§4) and their generalizations (§5) are discussed, including their energetic properties (§6). A case study on the clipping stage from a modified Ibanez Tube Screamer circuit is given (§7) and aspects of the original derivation (which we also use) are clarified (§8). §9 concludes.

2. PREVIOUS WORK

Early literature [4–7], Alfred Fettweis' classic article [2], and recent treatments [8, 9] give full reviews of WDF principles. For reviews on issues of topology and multiple/multiport nonlinearities, see recent work (which also proposes remedies) by Werner *et al.* [10–12] and Bernardini *et al.* [13–15]. We review only the history of *one-port nonlinearities* in WDFs.

A WDF can accommodate a single nonlinearity at the top of a tree structure [16]. Meerkötter and Scholz's study of ideal diodes and piecewise linear resistances first considered one-port WDF nonlinearities [17]. Felderhoff built on their work, accommodating nonlinear capacitors and inductors [18,19], and Sarti and De Poli used the *mutator* concept from classical network theory to formalize the study of nonlinear reactances alongside adaptors "with memory" [20, 21].

Meanwhile, researchers including Pedersini *et al.* [22, 23], De Sanctis *et al.* [24, 25], and Bilbao *et al.* [26, 27] were grafting WDF models of one-port nonlinear *mechanical* systems onto digital waveguide networks [1, 28, 29]. This trend continued in the *block-based modeling* research thread, e.g., [30–33].

In certain reference circuits, the restriction to a single nonlinear element can be circumvented by combining nonlinear elements into a one-port. Yeh and Smith solved an implicit diode pair wave domain characteristic via numerical methods [34–36]. Paiva *et al.* derived a simplified yet explicit wave-domain description for a diode pair using the Lambert $\mathcal{W}$ function, considering also semi-explicit methods for computing the Lambert $\mathcal{W}$ [3, 37]. In audio, an obvious application for these diode arrangements is WDF models of guitar distortion circuits—in fact Paiva *et al.* give two such case studies, on the Tube Screamer clipping stage and a Marshall preamplifier.

Guitar distortion[1] pedals often use antiparallel arrangements of diodes called "diode clippers." Single or multiple diodes are found in each direction in stock guitar pedals; adding or removing diodes is common in aftermarket modifications. Diode clippers have been extensively studied in VA [3, 12, 34–51], including complementary "black-box" (model identification) studies of distortion [1, 41, 52, 53][2].

[1] Sometimes pedals are classified as "overdrive" when the diode clipper is found in the feedback path of an active filter stage and as "distortion" otherwise [38].

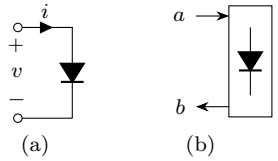

Fig. 1: Diode in (a) Kirchhoff and (b) wave domains.

2.1. Single Diode

A single diode, as shown in Fig. 1a, is modeled in the Kirchhoff domain by the Shockley ideal diode model

$$i = I_s \left(e^{v/V_T} - 1 \right), \tag{1}$$

where i is the current through and v the voltage across the diode, I_s is the reverse-bias saturation current, and V_T is the thermal voltage [54, 55].[3] We consider only instantaneous algebraic nonlinearities of the form $i = f(v)$ (or $b = f(a)$ in the wave domain); as such we omit time indices for compactness.

2.1.1. Wave domain

A wave (w) domain description can be found from the Kirchhoff (K) domain description (1) by using the standard WDF voltage wave definition. The voltage wave transformation and its inverse are

$$\text{K}\rightarrow\text{w:} \quad a = v + iR \quad , \quad b = v - iR \tag{2}$$

$$\text{w}\rightarrow\text{K:} \quad v = \tfrac{1}{2}a + \tfrac{1}{2}b \quad , \quad i = \tfrac{1}{2R}a - \tfrac{1}{2R}b, \tag{3}$$

where a and b are incident and reflected waves [2].

In theory, port resistance R in (2)–(3) is a completely arbitrary quantity. However, in practice the collection of diodes will always be at the root of a WDF tree [9, 16], so R will be prescribed by the port resistance of the tree below for realizability reasons.

Plugging (3) into (1) yields an implicit equation:

$$\tfrac{a-b}{2R} = I_s \left(e^{\frac{a+b}{2V_T}} - 1 \right). \tag{4}$$

An explicit wave domain equation would give b as a function of a. To derive one, we rearrange (4) using the Lambert $\mathcal{W}$ equation.

[2] `https://ccrma.stanford.edu/~jos/pasp/Nonlinear_Distortion.html`

[3] Often V_T is multiplied by an "ideality factor" n or η. In this work we omit the ideality factor for compactness.

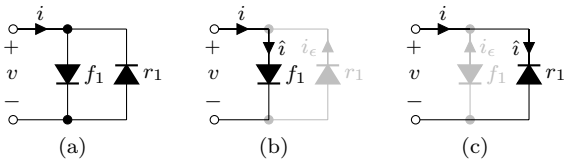

Fig. 2: (a) Diode pair, assuming (b) only forward diode f_1 or (c) only reverse diode r_1 conducts. Here and later in Fig. 4, neglected diodes are grayed out.

2.1.2. Lambert $\mathcal{W}$ function

The Lambert $\mathcal{W}$ function $\mathcal{W}(x)$ has been used previously in VA [13, 56, 57] and for many other applications [58]. The Lambert $\mathcal{W}$ function can be used to solve equations in one of these forms [58, 59]

$$\ln(A + Bx) + Cx = \ln(D) \tag{5}$$

$$(A + Bx)\, e^{Cx} = D \tag{6}$$

using

$$x = \tfrac{1}{C}\mathcal{W}\Big(\tfrac{CD}{B} e^{AC/B}\Big) - \tfrac{A}{B}. \tag{7}$$

To use this, we reframe (4) in the form of (6):

$$(a + 2RI_s - b)\, e^{-\frac{1}{2V_T}b} = 2RI_s e^{\frac{a}{2V_T}}. \tag{8}$$

The coefficients of (6), with $x = b$, are:

$$\begin{cases} A = a + 2RI_s & , \quad B = -1 \\ C = -\frac{1}{2V_T} & , \quad D = 2RI_s e^{\frac{a}{2V_T}}. \end{cases} \tag{9}$$

Plugging (9) into (7) yields

$$b = a + 2RI_s - 2V_T \mathcal{W}\Big(\tfrac{RI_s}{V_T} e^{\frac{a+RI_s}{V_T}}\Big), \tag{10}$$

an explicit wave domain equation; see also Fig. 1b.

2.2. Diode Pair

Two antiparallel diodes ("forward" f_1 and "reverse" r_1) are modeled in the Kirchhoff domain by

$$i = \underbrace{I_s\left(e^{v/V_T} - 1\right)}_{\text{current through } f_1} - \underbrace{I_s\left(e^{-v/V_T} - 1\right)}_{\text{current through } r_1} \tag{11}$$

and shown in Fig. 2a.[4]

[4] In this work, we assume that all diodes are matched, i.e., they share the same V_T and I_s.

Plugging the voltage wave definition (3) into (11) yields an implicit a–b relationship:

$$\tfrac{a-b}{2R} = \underbrace{I_s\left(e^{\frac{a+b}{2V_T}} - 1\right)}_{\text{from } f_1} - \underbrace{I_s\left(e^{-\frac{a+b}{2V_T}} - 1\right)}_{\text{from } r_1}. \tag{12}$$

Paiva *et al.* introduce the assumption that, depending on $\operatorname{sgn}(v)$, the terms due to f_1 or r_1 will dominate, i.e., only the conduction of one diode is considered at a time as shown in Fig. 2b–2c [3]. This assumption yields equations in the Kirchhoff domain

$$\hat{\imath} = \lambda I_s\left(e^{\frac{\lambda v}{V_T}} - 1\right) \quad \text{with} \quad \lambda = \operatorname{sgn}(v) \tag{13}$$

and the wave domain

$$\tfrac{\hat{a}-\hat{b}}{2R} = \hat{\lambda} I_s\left(e^{\hat{\lambda}\frac{\hat{a}+\hat{b}}{2V_T}} - 1\right) \quad \text{with} \quad \hat{\lambda} = \operatorname{sgn}(\hat{a}), \tag{14}$$

where sgn() is the *signum* function

$$\operatorname{sgn}(x) = \begin{cases} -1 & , \quad x < 0 \\ 0 & , \quad x = 0 \\ +1 & , \quad x > 0. \end{cases} \tag{15}$$

In [3], $\lambda = \operatorname{sgn}(v)$ is replaced by $\hat{\lambda} = \operatorname{sgn}(\hat{a})$ partway through the derivation, without comment. We will study conditions on this equivalence in §8. For now, at least for diode pairs and generalizations thereof, we assume that $\lambda = \hat{\lambda}$.

As before, we can rearrange (14) in the form of (6)

$$(\hat{a} + 2\hat{\lambda}RI_s - \hat{b}) e^{-\frac{\hat{\lambda}}{2V_T}\hat{b}} = 2\hat{\lambda}RI_s e^{\frac{\hat{\lambda}\hat{a}}{2V_T}}, \tag{16}$$

showing that we have (6) coefficients of

$$\begin{cases} A = \hat{a} + 2\hat{\lambda}RI_s & , \quad B = -1 \\ C = -\frac{\hat{\lambda}}{2V_T} & , \quad D = 2\hat{\lambda}RI_s e^{\frac{\hat{\lambda}\hat{a}}{2V_T}}. \end{cases} \tag{17}$$

Hence the Lambert $\mathcal{W}$ function rearranges (14) to

$$\hat{b} = \hat{a} + 2\hat{\lambda}\left[RI_s - V_T \mathcal{W}\Big(\tfrac{RI_s}{V_T} e^{\frac{\hat{\lambda}\hat{a}+RI_s}{V_T}}\Big)\right], \tag{18}$$

which is equivalent[5] to the results of Paiva *et al.* [3]

$$\hat{b} = \operatorname{sgn}(\hat{a})\left[|\hat{a}| + 2RI_s - 2V_T \mathcal{W}\Big(\tfrac{RI_s}{V_T} e^{\frac{|\hat{a}|+RI_s}{V_T}}\Big)\right]. \tag{19}$$

[5] Using our notation however, i.e., dropping n and including hats to make the approximation clear.

(18)–(19) give $\hat{b} = f(\hat{a})$. These are actually *exact* relationships between $\hat{a}$ and $\hat{b}$. However, since a WDF tree delivers a (not $\hat{a}$) to the nonlinear root, these are used as $\hat{b} = f(a)$. Hence, the wave-domain equation describing the diode pair is rendered explicit with the Lambert $\mathcal{W}$ function at the cost of approximation error due to the neglected diode.

3. ALTERNATIVE SIMPLIFICATION

In this section, we propose an alternate to §2.2. Noticing that the -1 terms in (11) cancel yields

$$i = \underbrace{I_s e^{v/V_T}}_{\text{from } f_1} - \underbrace{I_s e^{-v/V_T}}_{\text{from } r_1}, \tag{20}$$

or equivalently in the wave domain

$$\tfrac{a-b}{2R} = \underbrace{I_s e^{\frac{a+b}{2V_T}}}_{\text{from } f_1} - \underbrace{I_s e^{-\frac{a+b}{2V_T}}}_{\text{from } r_1}. \tag{21}$$

Assuming that the f_1 or r_1 term dominates yields

$$\hat{\imath} = \lambda I_s e^{\lambda v/V_T} \quad \text{with} \quad \lambda = \operatorname{sgn}(v). \tag{22}$$

Plugging in (3) yields

$$\tfrac{\hat{a}-\hat{b}}{2R} = \hat{\lambda} I_s e^{\frac{\hat{\lambda}(\hat{a}+\hat{b})}{2V_T}} \quad \text{with} \quad \hat{\lambda} = \operatorname{sgn}(a). \tag{23}$$

As before, we can reframe (23) in the form of (6)

$$(\hat{a} - \hat{b}) e^{-\frac{\hat{\lambda}}{2V_T}\hat{b}} = 2\hat{\lambda} R I_s e^{\frac{\hat{\lambda}\hat{a}}{2V_T}}, \tag{24}$$

with (6) coefficients

$$\begin{cases} A = \hat{a} & , \quad B = -1 \\ C = -\frac{\hat{\lambda}}{2V_T} & , \quad D = 2\hat{\lambda} R I_s e^{\frac{\hat{\lambda}\hat{a}}{2V_T}}. \end{cases} \tag{25}$$

Hence the Lambert $\mathcal{W}$ function rearranges (23) to:

$$\hat{b} = \hat{a} - 2\hat{\lambda} V_T \mathcal{W}\!\left(\tfrac{R I_s}{V_T} e^{\frac{\hat{\lambda}\hat{a}}{V_T}} \right) \text{ with } \hat{\lambda} = \operatorname{sgn}(\hat{a}). \tag{26}$$

Again, this is an exact relationship between $\hat{b}$ and $\hat{a}$; using it as $\hat{b} = f(a)$ introduces approximation error.

4. IMPROVED MODEL

Continuing from §3, where we considered the actual current i and the approximate current $\hat{\imath}$, we now consider the *current error* i_ϵ. We define:

$$i = \hat{\imath} - i_\epsilon \quad \longleftrightarrow \quad i_\epsilon = \hat{\imath} - i. \tag{27}$$

Considering (20) and (22) in light of (27) yields

$$i_\epsilon = \lambda I_s e^{-\lambda v/V_T} \quad \text{with} \quad \lambda = \operatorname{sgn}(v). \tag{28}$$

Plugging (3) into (28) yields

$$\tfrac{a_\epsilon - b_\epsilon}{2R} = \hat{\lambda} I_s e^{-\frac{\hat{\lambda}(a_\epsilon + b_\epsilon)}{2V_T}} \quad \text{with} \quad \hat{\lambda} = \operatorname{sgn}(a). \tag{29}$$

As before, (29) can be rearranged in the form of (6)

$$(a_\epsilon - b_\epsilon) e^{\frac{\hat{\lambda}}{2V_T} b_\epsilon} = 2\hat{\lambda} R I_s e^{-\frac{\hat{\lambda} a_\epsilon}{2V_T}}, \tag{30}$$

showing that we have (6) coefficients of

$$\begin{cases} A = a_\epsilon & , \quad B = -1 \\ C = \frac{\hat{\lambda}}{2V_T} & , \quad D = 2\hat{\lambda} R I_s e^{-\frac{\hat{\lambda} a_\epsilon}{2V_T}}. \end{cases} \tag{31}$$

Hence the Lambert $\mathcal{W}$ function rearranges (29) to:

$$b_\epsilon = a_\epsilon + 2\hat{\lambda} V_T \mathcal{W}\!\left(-\tfrac{R I_s}{V_T} e^{-\hat{\lambda} a_\epsilon / V_T} \right). \tag{32}$$

We have studied Kirchhoff-domain equations that find i from v (20), $\hat{\imath}$ from v (22), and i_ϵ from v (28). If these relationships are considered as *vectors* $\begin{pmatrix} v & i \end{pmatrix}$, $\begin{pmatrix} v & \hat{\imath} \end{pmatrix}$, and $\begin{pmatrix} v & i_\epsilon \end{pmatrix}$ stretching from the origin on the v–i plane, the following vector equation applies:

$$\begin{pmatrix} v & i \end{pmatrix} = \begin{pmatrix} v & \hat{\imath} \end{pmatrix} - \begin{pmatrix} v & i_\epsilon \end{pmatrix} + \begin{pmatrix} v & 0 \end{pmatrix}. \tag{33}$$

The wave-domain counterpart to $\begin{pmatrix} v & 0 \end{pmatrix}$ is found by realizing its equivalence to $i = 0$ and plugging in (3):

$$\tfrac{a_v - b_v}{2R} = 0 \quad \longrightarrow \quad b_v = a_v. \tag{34}$$

At the same time, in hope of finding some function $b = f(a)$, we have derived wave-domain equations which find $\hat{b}$ from $\hat{a}$ (26), b_ϵ from a_ϵ (32), and now b_v from a_v (34). Again, we consider these relationships as vectors, this time stretching from the origin on the a–b plane: $\begin{pmatrix} a & b \end{pmatrix}$, $\begin{pmatrix} \hat{a} & \hat{b} \end{pmatrix}$, $\begin{pmatrix} a_\epsilon & b_\epsilon \end{pmatrix}$, and $\begin{pmatrix} a_v & b_v \end{pmatrix}$.

Since the voltage wave transformation (2) is linear, (33) applies on the wave plane as well:

$$\begin{pmatrix} a & b \end{pmatrix} = \begin{pmatrix} \hat{a} & \hat{b} \end{pmatrix} - \begin{pmatrix} a_\epsilon & b_\epsilon \end{pmatrix} + \begin{pmatrix} a_v & b_v \end{pmatrix}. \tag{35}$$

Summing the a components of (35) yields

$$a = \operatorname{proj}_a\!\begin{pmatrix} a & b \end{pmatrix} = \hat{a} - a_\epsilon + a_v. \tag{36}$$

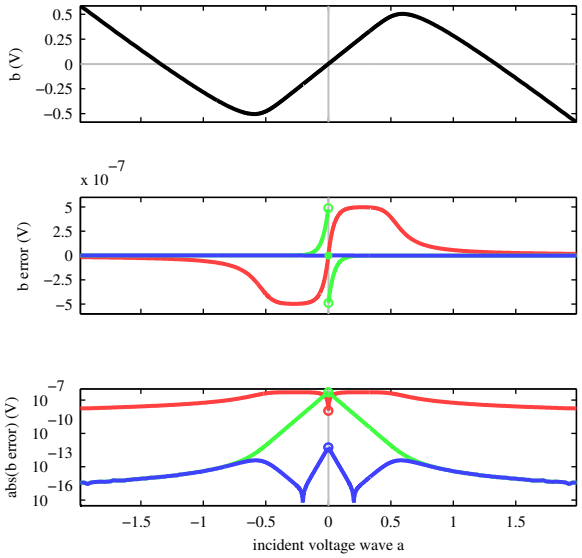

Fig. 3: Comparing diode clipper models: a–b characteristic (top), error in b for different models (Red: Paiva, Green: Alternative, Blue: Improved), and absolute value of error in b on log scale (bottom).

Summing the b components of (35) yields

$$b = \text{proj}_b(a \quad b) = \hat{b} - b_\epsilon + b_v \tag{37}$$

$$b = \hat{a} - a_\epsilon + a_v - 2\hat{\lambda}V_T\mathcal{W}\left(\frac{RI_s}{V_T}e^{\hat{\lambda}\hat{a}/V_T}\right) - 2\hat{\lambda}V_T\mathcal{W}\left(-\frac{RI_s}{V_T}e^{-\hat{\lambda}a_\epsilon/V_T}\right). \tag{38}$$

Unfortunately (36) and (38) do not depend only on a, but also on $\hat{a}$, a_ϵ, and a_v.

Now, we introduce a simplification that renders (38) tractable. Recalling the voltage wave definition (2), we see that when $i \ll v$, $a \approx v$. Recalling (20), (22), and (28)—since $i \ll v$ near $v = 0$, we can see that near $v = 0$, $a \approx \hat{a} \approx a_\epsilon \approx a_v$. Making this assumption on (38) yields our improved model:

$$\tilde{b} = a - 2\hat{\lambda}V_T\left[\mathcal{W}\left(\frac{RI_s}{V_T}e^{\frac{\hat{\lambda}a}{V_T}}\right) + \mathcal{W}\left(-\frac{RI_s}{V_T}e^{-\frac{\hat{\lambda}a}{V_T}}\right)\right], \tag{39}$$

where $\tilde{b} \approx b$. Another way to think about this correction term is that the original model is very good far from $a = 0$. Around $a = 0$ the assumption used to derive the correction factor ($a \approx \hat{a} \approx a_\epsilon \approx a_v$) is valid. When $|a| \gg 0$, the assumptions used to derive the correction factor become less valid, but the value of the correction factor also approaches zero, and the original equation was already very accurate.

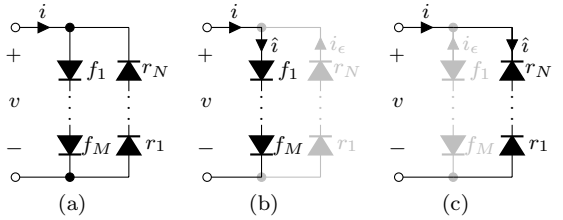

Fig. 4: (a) Diode pair generalization, with M forward and N reverse diodes, assuming (b) only forward diodes or (c) only reverse diodes conduct.

We might think of applying the same reasoning to improve the original Paiva *et al.* model. However, the justification for the final step would be poor, and the derivation would not yield improvements.

A comparison among the Paiva *et al.*, alternative, and improved models is shown in Fig. 3, using a port resistance of $R = 100\ \Omega$ for legibility reasons only. The middle panel shows how far each model is from the ground truth, which is tabulated in the Kirchhoff domain and transformed via (3). It is clear that the alternative model has less error than the Paiva *et al.* model and that the improved model has even less error still. In fact, the improved model error is only visible against the others on a log scale (bottom panel); across most of the incident wave range it has many orders of magnitude less approximation error.

5. GENERALIZATIONS

We generalize the models discussed so far by considering the case where the forward diode f_1 is replaced by M forward diodes $f_1 \dots f_M$ in series and the reverse diode r_1 is replaced by N reverse diodes $r_1 \dots r_N$ in series. This class of clippers is common in stock guitar distortion pedals and aftermarket modifications. This generalized arrangement is shown in Fig. 4 and modeled in the Kirchhoff domain by:

$$i = \underbrace{I_s\left(e^{\frac{v}{MV_T}} - 1\right)}_{\text{from } f_1 \dots f_M} - \underbrace{I_s\left(e^{-\frac{v}{NV_T}} - 1\right)}_{\text{from } r_1 \dots r_N} \tag{40}$$

and, substituting (3), in the wave domain by

$$\frac{a-b}{2R} = \underbrace{I_s\left(e^{\frac{a+b}{2MV_T}} - 1\right)}_{\text{from } f_1 \dots f_M} - \underbrace{I_s\left(e^{-\frac{a+b}{2NV_T}} - 1\right)}_{\text{from } r_1 \dots r_N} \tag{41}$$

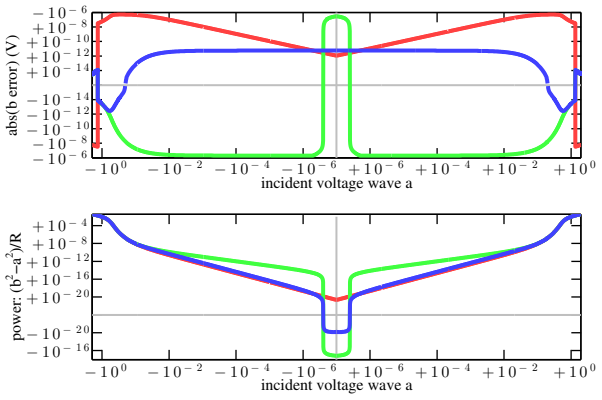

Fig. 5: Energetic investigation, including incremental approximation error power (top) and total power (bottom). Axes are on pseudo-log scales, with small values clipped below thresholds, colors as in Fig. 3.

or, letting the -1 terms cancel,

$$\frac{a-b}{2R} = \underbrace{I_s e^{\frac{a+b}{2MV_T}}}_{f_1 \dots f_M} - \underbrace{I_s e^{-\frac{a+b}{2NV_T}}}_{r_1 \dots r_N}. \tag{42}$$

Generalizing the techniques presented throughout this paper is straightforward; for brevity the details are omitted and only the results are reported below.

Taking the approach of Paiva *et al.* [3] yields

$$b = a + 2\lambda \left[RI_s - \mu_0 V_T \mathcal{W}\left(\frac{RI_s}{\mu_0 V_T} e^{\frac{\lambda a + RI_s}{\mu_0 V_T}} \right) \right]. \tag{43}$$

Letting the -1 terms cancel and following the alternative simplification procedure of §3 yields

$$b = a - 2\lambda\mu_0 V_T \mathcal{W}\left(\frac{RI_s}{\mu_0 V_T} e^{\frac{\lambda a}{\mu_0 V_T}} \right). \tag{44}$$

Improving the alternative simplification with a second Lambert $\mathcal{W}$ term as in §4 yields

$$b = a - 2\lambda V_T \left[\mu_0 \mathcal{W}\left(\frac{RI_s}{\mu_0 V_T} e^{\frac{\lambda a}{\mu_0 V_T}} \right) + \mu_1 \mathcal{W}\left(-\frac{RI_s}{\mu_1 V_T} e^{-\frac{\lambda a}{\mu_1 V_T}} \right) \right]. \tag{45}$$

For these three models (43)–(45), factors μ_0 and μ_1 account for the M forward and N reverse diodes:

$$\mu_0 = \begin{cases} M\ , & a \geq 0 \\ N\ , & a < 0 \end{cases} \quad \text{and} \quad \mu_1 = \begin{cases} N\ , & a \geq 0 \\ M\ , & a < 0. \end{cases} \tag{46}$$

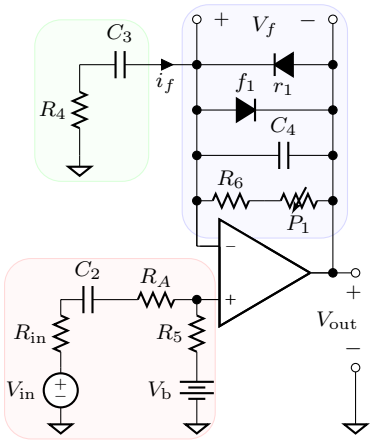

Fig. 6: Tube Screamer clipping stage circuit, with output voltage found by $V_{\text{out}} = V_+ + V_f$.

comp.	value	comp.	value
R_{in}	1 Ω	V_b	4.5 V
R_A	220 Ω	C_2	1 μF
R_4	4.7 kΩ	C_3	0.047 μF
R_5	10 kΩ	C_4	51 pF
R_6	51 kΩ	f_1	1N914
P_1	0–500 kΩ	r_1	1N914

Table 1: Clipping stage component electrical values.

6. ENERGETIC PROPERTIES

The original linear WDF formulation [2, 4, 5] relied on energetic interpretations of numerical error; numerical operations were guaranteed to correspond to *passive* reference domain processes, ensuring, e.g., good sensitivity and stability properties [6].

Werner and Smith similarly interpreted interpolation error in one-port nonlinear WDF lookup tables energetically, yielding recommendations for table formation and interpolation techniques [57]. In this framework, we study diode clipper models.

Fettweis gives an expression for the instantaneous (pseudo)power p absorbed at a WDF port as [6]:

$$p = \left(a^2 - b^2\right)/R. \tag{47}$$

In [57], Werner and Smith claimed that, in the context of linear interpolation, power interpolation error ϵ should fulfill $\epsilon \geq 0$ to ensure that interpolation approximation error does not correspond to creating energy in the reference domain. This yields a rela-

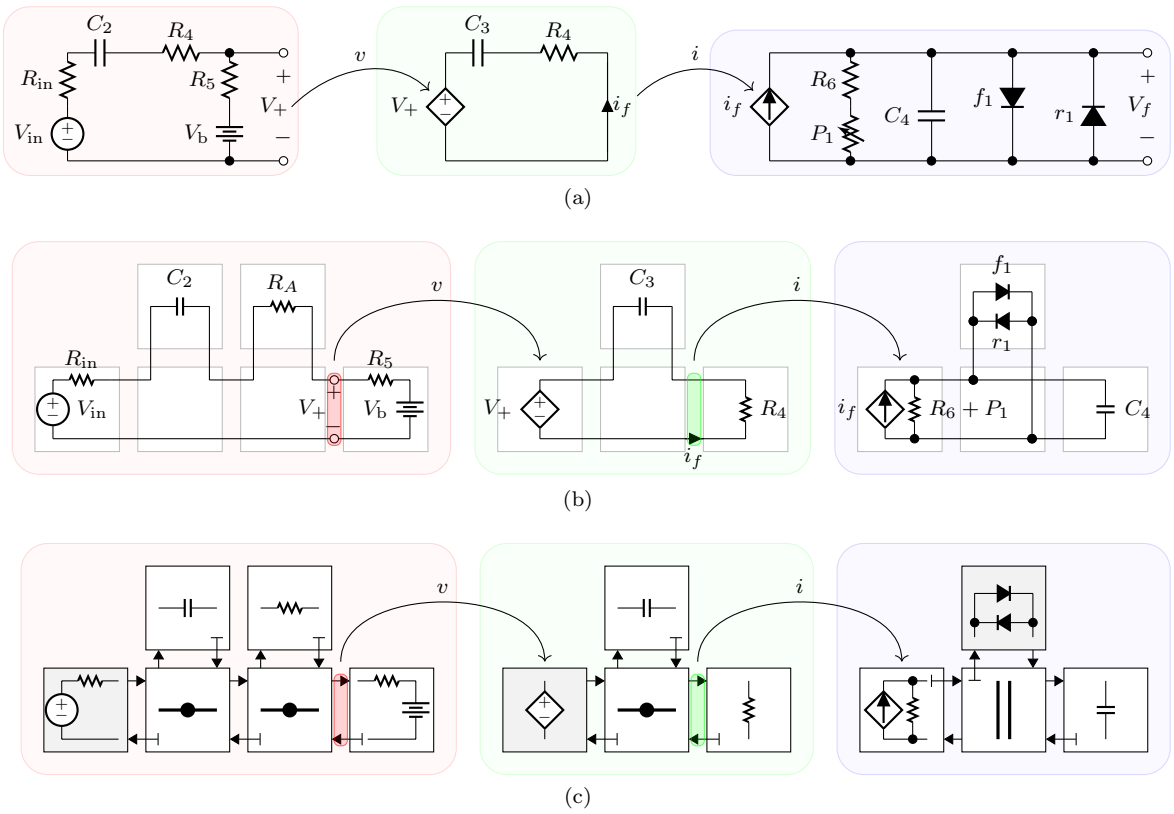

Fig. 7: (a) Equivalent circuit to Tube Screamer clipping stage (Fig. 6), (b) equivalent circuit rearranged to highlight WDF adaptor structure, and (c) corresponding WDF adaptor structure (root notes highlighted).

tionship $|\hat{b}| \leq |b|$. This is equivalent to satisfying:

$$|\hat{b}| - |b| \leq 0. \tag{48}$$

To determine whether the approximations discussed in this paper are also "energy-safe," we need to find out if (48) is satisfied. Without an exact equation $b = f(a)$, this can only be done experimentally, by transforming tabulated Kirchhoff-domain data into the wave domain by (3). In Fig. 5, we plot (48) for the Paiva *et al.* model, the alternative model, and the improved model. We can see that neither (48) nor $p \geq 0$ is satisfied for any of the models under the entire range of incident waves. Although we can not conclude that any model is superior on energetic grounds, the energetic issues are very tiny in magnitude. None of the models seem to suffer from stability problems, etc., when applied to the following case study.

7. CASE STUDY

We apply our method to WDF modeling of a modded TS10 Tube Screamer clipping stage, with component names and values (Table 1) from [60, 61]. From the reference circuit (Fig. 6), a WDF model is created as in [3]. An equivalent circuit (Fig. 7a) is created by leveraging ideal op-amp laws, highlighting how the circuit can be seen as 3 sub-circuits with feedforward controlled sources. A rearranged version (Fig. 7b) highlights a portwise interpretation, from which the WDF structure follows directly (Fig. 7c), with the controlled sources implemented as tree–tree cross-controls [9].

WDF simulations that use the improved diode clipper model with various numbers of forward and reverse diodes are shown in Fig. 8. In all cases, agreement with SPICE [62] simulations demonstrates the validity of the improved WDF model.

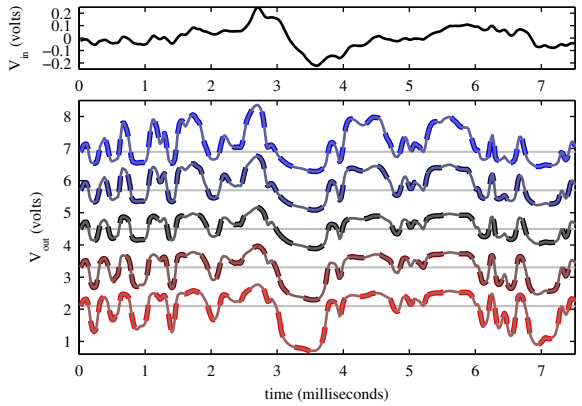

Fig. 8: Comparing WDF (solid) and SPICE (thick dashed) simulations (bottom) of the Tube Screamer clipping stage in response to a guitar input signal (top), with various values of M and N. From top to bottom: $M = 3$ and $N = 1$ (blue), $M = 2$ and $N = 1$ (dark blue), $M = 1$ and $N = 1$ (black), $M = 1$ and $N = 2$ (dark red), $M = 1$ and $N = 3$ (red). Cases other than $M = 1$ and $N = 1$ (black) are offset for legibility; in all cases the gray horizontal line indicates the 4.5 V bias voltage as a reference.

8. COMMENTS ON DERIVATION

Let us reconsider the properties $\lambda = \text{sgn}(v)$ and $\hat{\lambda} = \text{sgn}(a)$. In this work and [3], the assumption

$$\lambda = \hat{\lambda} \tag{49}$$

is needed. It is clear from the voltage wave definition (2) that, *in general*, $\text{sgn}(v) \neq \text{sgn}(a)$ and hence $\lambda \neq \hat{\lambda}$. However, for the case of an antiparallel diode pair and generalizations thereof, (49) is true. We present two proofs: a geometric proof (§8.1) and an algebraic proof by contradiction (§8.2).

8.1. Geometric Proof

(2) is written in matrix form as:

$$\begin{bmatrix} a \\ b \end{bmatrix} = \begin{bmatrix} 1 & R \\ 1 & -R \end{bmatrix} \begin{bmatrix} v \\ i \end{bmatrix}. \tag{50}$$

We can consider this as a move from the v–i to the a–b plane. QR decomposition gives the transformation matrix $\left[\begin{smallmatrix} 1 & R \\ 1 & -R \end{smallmatrix}\right]$ a geometric interpretation.

In general, QR decomposition breaks a square matrix $\mathbf{A}$ into a product of orthogonal matrix $\mathbf{Q}$ (i.e., $\mathbf{Q}^\mathsf{T}\mathbf{Q} = \mathbf{I}$) and upper-triangular matrix $\mathbf{R}$. In the general 2×2 case, $\mathbf{A} = \mathbf{QR}$ can be written [63]:

$$\underbrace{\begin{bmatrix} \alpha & \beta \\ \gamma & \delta \end{bmatrix}}_{\mathbf{A}} = \underbrace{\begin{bmatrix} \cos\theta & -\sin\theta \\ \sin\theta & \cos\theta \end{bmatrix}}_{\mathbf{Q}} \underbrace{\begin{bmatrix} x & z \\ 0 & y \end{bmatrix}}_{\mathbf{R}}. \tag{51}$$

We can find θ, x, y, and z in (51) analytically from α, β, γ, and δ. With $\theta = \text{atan}(\alpha/\gamma)$, we find

$$\mathbf{Q} = \begin{bmatrix} \frac{\alpha}{\zeta} & -\frac{\gamma}{\zeta} \\ \frac{\gamma}{\zeta} & \frac{\alpha}{\zeta} \end{bmatrix}, \quad \mathbf{R} = \begin{bmatrix} \zeta & \frac{\alpha\beta+\gamma\delta}{\zeta} \\ 0 & \frac{\alpha\delta-\beta\gamma}{\zeta} \end{bmatrix}, \tag{52}$$

with $\zeta = \sqrt{\alpha^2 + \gamma^2}$. Plugging (50) (i.e., $\left[\begin{smallmatrix} \alpha & \beta \\ \gamma & \delta \end{smallmatrix}\right] = \left[\begin{smallmatrix} 1 & R \\ 1 & -R \end{smallmatrix}\right]$) into (52) yields

$$\mathbf{Q} = \begin{bmatrix} \frac{1}{\sqrt{2}} & -\frac{1}{\sqrt{2}} \\ \frac{1}{\sqrt{2}} & \frac{1}{\sqrt{2}} \end{bmatrix}, \quad \mathbf{R} = \begin{bmatrix} \sqrt{2} & 0 \\ 0 & -\sqrt{2}R \end{bmatrix}. \tag{53}$$

Hence, we can interpret a transformation from the v–i plane to the a–b plane as a stretch by $\sqrt{2}$ in the v direction and $-\sqrt{2}R$ in the i direction (via matrix $\mathbf{R}$), followed by a $\theta = -\pi/4$ rotation (via matrix $\mathbf{Q}$).

(49) is satisfied in quadrants I and III on the v–i plane, which also contain the entire generalized diode clipper curve. Hence, by the stretch and rotation the curves still lie in regions that satisfy (49) on the a–b plane.

8.2. Proof by Contradiction

Assume a point $\begin{pmatrix} \mathcal{A} & \mathcal{B} \end{pmatrix}$ is on the diode curve (42) and also is in a region where (49) is not true, i.e.:

$$\mathcal{A} \lesseqgtr 0 \quad \text{and} \quad \mathcal{A} \gtreqless -\mathcal{B}. \tag{54}$$

Without loss of generality, we can say that $\mathcal{A}$ is greater (less) than $-\mathcal{B}$ by a positive offset k:

$$\mathcal{A} = -\mathcal{B} \pm k \quad \text{or} \quad \mathcal{B} = -\mathcal{A} \pm k \quad \text{with} \quad k > 0. \tag{55}$$

Plugging (55) into (42) yields

$$\frac{2\mathcal{A} \mp k}{2R} = I_s \left(e^{\pm \frac{k}{2MV_T}} - e^{\mp \frac{k}{2NV_T}} \right). \tag{56}$$

Due to the constraint (55), the left side of (56) is negative (positive). Since $k, I_s, M, N, V_T > 0$, the right side of (56) is positive (negative). Therefore we have a contradiction: no point may ever satisfy both (42) and (54). Therefore for (42), (49) is true.

9. CONCLUSION

By deriving improved and generalized wave-domain expressions for the types of diode clippers that are common in guitar distortion circuits, this work adds to the toolkit of WDF algorithm designers.

Because the improvement over the Paiva *et al.* and alternative models is small with respect to existing systematic error in the WDFs (e.g. aliasing, frequency warping) and the SPICE simulation cannot be taken completely as a ground truth (due to foibles of automatic time-step control and global iterative convergence), the alternative and improved models cannot be justified by showing a closer fit between the WDF and SPICE. We can only reason that the alternative and improved models intrinsically have less approximation error than the Paiva *et al.* model.

We hope that this work can inform future work on decreasing approximation error in the case of multiport nonlinearities [13], where issues of approximation error and its energetic interpretation may be more significant.

ACKNOWLEDGMENTS

Thanks to François Germain and Jonathan Abel for key discussions and to the anonymous reviewers.

10. REFERENCES

[1] J. O. Smith III, *Physical Audio Signal Processing for Virtual Musical Instruments and Audio Effects*, online book, 2010 edition.

[2] A. Fettweis, "Wave digital filters: Theory and practice," *Proc. IEEE*, vol. 74, no. 2, pp. 270–327, 1986.

[3] R. C. D. de Paiva, S. D'Angelo, J. Pakarinen, and V. Välimäki, "Emulation of operational amplifiers and diodes in audio distortion circuits," *IEEE Trans. Circuits Syst. II: Expr. Briefs*, vol. 59, no. 10, 2012.

[4] A. Fettweis, "Some principles of designing digital filters imitating classical filter structures," *IEEE Trans. Circuit Theory*, vol. 18, no. 2, pp. 314–316, 1971.

[5] A. Fettweis, "Digital filters structures related to classical filter networks," *Archiv fur Elektronik und Übertragungstechnik*, vol. 25, pp. 79–89, 1971.

[6] A Fettweis, "Pseudo-passivity, sensitivity, and stability of wave digital filters," *IEEE Trans. Circuit Theory*, vol. 19, no. 6, pp. 668–673, 1972.

[7] A. Fettweis and K. Meerkötter, "On adaptors for wave digital filters," *IEEE Trans. Acoust., Speech, Signal Process.*, vol. 23, no. 6, pp. 516–525, 1975.

[8] S. Bilbao, *Wave and Scattering Methods for Numerical Simulation*, John Wiley & Sons, New York, July 2004.

[9] G. De Sanctis and A. Sarti, "Virtual analog modeling in the wave-digital domain," *IEEE Trans. Audio, Speech, Language Process.*, vol. 18, no. 4, pp. 715–727, 2010.

[10] K. J. Werner, V. Nangia, J. O. Smith III, and J. S. Abel, "A general and explicit formulation for wave digital filters with multiple/multiport nonlinearities and complicated topologies," in *IEEE Workshop Appl. Signal Process. Audio Acoust.*, New Paltz, NY, Oct. 18–21 2015.

[11] K. J. Werner, J. O. Smith III, and J. S. Abel, "Wave digital filter adaptors for arbitrary topologies and multiport linear elements," submitted to DAFx 2015.

[12] K. J. Werner, V. Nangia, J. O. Smith III, and J. S. Abel, "Resolving wave digital filters with multiple/multiport nonlinearities," submitted to DAFx 2015.

[13] A. Bernardini, "Modeling nonLinear circuits with multiport elements in the wave digital domain," M.S. thesis, Politecnico di Milano, Italy, Apr. 2015.

[14] A. Bernardini, K. J. Werner, A. Sarti, and J. O. Smith III, "Multi-port nonlinearities in wave digital structures," in *Proc. IEEE Int. Symp. Signals, Circuits, Syst. (ISSCS 2015)*, Iași, Romania, July 9–10 2015.

[15] A. Bernardini, K. J. Werner, A. Sarti, and J. O. Smith III, "Modeling a class of multi-port nonlinearities in wave digital structures," in *Proc. European Signal Process. Conf. (EUSIPCO)*, Nice, France, Aug. 31 – Sept. 4 2015.

[16] A. Sarti and G. De Sanctis, "Systematic methods for the implementation of nonlinear wave-digital structures," *IEEE Trans. Circuits Syst. I: Reg. Papers*, vol. 56, no. 2, pp. 460–472, 2009.

[17] K. Meerkötter and R. Scholz, "Digital simulation of nonlinear circuits by wave digital filter principles," in *IEEE Int. Symp. Circuits Syst.*, June 1989, vol. 1, pp. 720–723.

[18] T. Felderhoff, "Simulation of nonlinear circuits with period doubling and chaotic behavior by wave digital filter principles," *IEEE Trans. Circuits Syst. I: Fundam. Theory Appl.*, vol. 41, no. 7, pp. 485–491, 1994.

[19] T. Felderhoff, "A new wave description for nonlinear elements," in *Proc. IEEE Int. Symp. Circuits Syst.*, Sept. 1996, vol. 3, pp. 221–224.

[20] A. Sarti and G. De Poli, "Generalized adaptors with memory for nonlinear wave digital structures," in *Proc. European Signal Process. Conf.*, Sept. 1996, vol. 3.

[21] A. Sarti and G. De Poli, "Toward nonlinear wave digital filters," *IEEE Trans. Signal Process.*, vol. 47, no. 6, 1999.

[22] F. Pedersini, A. Sarti, and S. Tubaro, "Block-wise physical model synthesis for musical acoustics," *Electron. Lett.*, vol. 35, no. 17, pp. 1418–1419, 1999.

[23] F. Pedersini, A. Sarti, and S. Tubaro, "Object-based sound synthesis for virtual environments using musical acoustics," *IEEE Signal Process. Mag.*, vol. 17, no. 6, pp. 37–51, Nov. 2000.

[24] G. De Sanctis, "Una nuova metodologia per l'implementazione automatica di strutture ad onda numerica orientata alla modellazione ad oggetti di interazioni acustiche," M.S. thesis, Politecnico di Milano, Italy, 2002.

[25] G. De Sanctis, A. Sarti, and S. Tubaro, "Automatic synthesis strategies for object-based dynamical physical models in musical acoustics," in *Proc. Int. Conf. Digital Audio Effects*, London, UK, Sept. 8–11 2003, vol. 6.

[26] S. D. Bilbao, J. Bensa, R. Kronland-Martinet, and J. O. Smith III, "The wave digital piano hammer: a passive formulation," in *Proc. Meeting Acoust. Soc. Amer.*, Cancun, Mexico, 2002, vol. 114.

[27] S. Bilbao, J. Bensa, and R. Kronland-Martinet, "The wave digital reed: A passive formulation," in *Proc. Int. Conf. Digital Audio Effects*, London, UK, 2003, vol. 6.

[28] J. O. Smith III, "Music applications of digital waveguides," CCRMA Tech. Rep. STAN-M-39, Stanford University, CA, May 19 1987.

[29] J. O. Smith III, "Physical modeling using digital waveguides," *Comput. Music J.*, vol. 16, no. 4, 1992.

[30] M. Karjalainen, "BlockCompiler: Efficient simulation of acoustic and audio systems," in *Proc. Audio Eng. Soc. Conv.*, Amsterdam, Netherlands, Mar. 2003, vol. 114.

[31] R. Rabenstein, S. Petrausch, A. Sarti, G. De Sanctis, C. Erkut, and M. Karjalainen, "Block-based physical modeling for digital sound synthesis," *IEEE Signal Process. Mag.*, pp. 42–54, Mar. 2007.

[32] M. Karjalainen, "Efficient realization of wave digital components for physical modeling and sound synthesis," *IEEE Trans. Audio, Speech, Language Process.*, vol. 16, no. 5, pp. 947–956, 2008.

[33] R. Rabenstein and S. Petrausch, "Block-based physical modeling with applications in musical acoustics," *Int. J. Appl. Math. Comput. Sci.*, vol. 18, no. 3, 2008.

[34] D. T.-M. Yeh and J. O. Smith III, "Simulating guitar distortion circuits using wave digital and nonlinear state-space formulations," *Proc. Int Conf. Digital Audio Effects (DAFx-08)*, pp. 19–26, 2008.

[35] D. Yeh, "Tutorial on wave digital filters," `https://ccrma.stanford.edu/~dtyeh/`, Jan. 25 2008.

[36] D. T.-M. Yeh, *Digital implementation of musical distortion circuits by analysis and simulation*, Ph.D. dissertation, Stanford University, CA, 2009.

[37] R. C. D. de Paiva, *Circuit modeling studies related to guitars and audio processing*, Ph.D. dissertation, Aalto University, Espoo, Finland, Sept. 2013.

[38] D. T.-M. Yeh, J. S. Abel, and J. O. Smith III, "Simplified, physically-informed models of distortion and overdrive guitar effects pedals," in *Proc. Int. Conf. Digital Audio Effects*, Bordeaux, France, Sept. 2007, pp. 189–196.

[39] D. T.-M. Yeh, J. S. Abel, and J. O. Smith III, "Simulation of the diode limiter in guitar distortion circuits by numerical solution of ordinary differential equations," in *Proc. Int. Conf. Digital Audio Effects (DAFx-10)*, Bordeaux, France, Sept. 10–15 2007, pp. 197–204.

[40] D. T.-M. Yeh, J. S. Abel, A. Vladimirescu, and J. O. Smith III, "Numerical methods for simulation of guitar distortion circuits," *Comput. Music J.*, vol. 32, no. 2, pp. 23–42, 2008.

[41] J. Pakarinen and D. T.-M. Yeh, "A review of digital techniques for modeling vacuum-tube guitar amplifiers," *Comput. Music J.*, vol. 33, no. 2, pp. 85–100, 2009.

[42] J. Macak and J. Schimmel, "Nonlinear circuit simulation using time-variant filter," in *Proc. Int. Conf. Digital Audio Effects (DAFx-12)*, York, UK, Sept. 17–21 2009.

[43] K. Dempwolf, M. Holters, and U. Zölzer, "Discretization of parametric analog circuits for real-time simulations," in *Proc. Int. Conf. Digital Audio Effects (DAFx-10)*, Granz, Austria, Sept. 6–10 2010, vol. 13.

[44] D. T.-M. Yeh, J. S. Abel, and J. O. Smith III, "Automated physical modeling of nonlinear audio circuits for real-time audio effects—part I: Theoretical development," *IEEE Trans. Audio, Speech, Language Process.*, vol. 18, no. 4, pp. 728–737, 2010.

[45] M. Holters, K. Dempwolf, and U. Zölzer, "A digital emulation of the Boss SD-1 Super Overdrive pedal based on physical modeling," in *Proc. Int. Audio Eng. Soc. Conv.*, New York, NY, Oct. 20–23 2011, vol. 131.

[46] F. G. Germain, J. S. Abel, P. Depalle, and M. M. Wanderley, "Uniform noise sequences for nonlinear system identification," in *Proc. Int. Conf. Digital Audio Effects (DAFx-12)*, York, UK, Sept. 17–21 2012, vol. 15.

[47] J. Mačák, *Real-Time Digital Simulation of Guitar Amplifiers as Audio Effects*, Ph.D. dissertation, Brno University of Technology, Czech Republic, 2012.

[48] P. R. Benois, "Simulation framework for analog audio circuits based on nodal DK method," M.S. thesis, Helmut Schmidt University, Hamburg, Germany, Dec. 2013.

[49] T. Schwerdtfeger and A. Kummert, "A multidimensional approach to wave digital filters with multiple nonlinearities," in *Proc. European Signal Process. Conf. (EUSIPCO)*, Lisbon, Portugal, Sept. 1–5 2014.

[50] K. J. Werner, J. S. Abel, and J. O. Smith III, "A physically-informed, circuit-bendable, digital model of the Roland TR-808 bass drum circuit," in *Proc. Int. Conf. Digital Audio Effects (DAFx-14)*, Erlangen, Germany, Sept. 1–5 2014, vol. 17.

[51] F. G. Germain and K. J. Werner, "Design principles for lumped model discretisation using Möbius transforms," submitted to DAFx 2015.

[52] C. R. Sullivan, "Extending the Karplus–Strong algorithm to synthesize electric guitar timbres with distortion and feedback," *Comput. Music J.*, vol. 14, no. 3, pp. 26–37, 1990.

[53] J. Timoney and V. Lazzarini, "Saturation non-linearities for virtual analog filters," in *Proc. Forum Acusticum*, Aalborg, Denmark, June/July 2011.

[54] W. Shockley, "The theory of p–n junctions in semiconductors and p–n junction transistors," *Bell Syst. Tech. J.*, vol. 28, no. 3, pp. 435–489, 1949.

[55] S. M. Sze, *Physics of Semiconductor Devices*, John Wiley & Sons, New York, 2nd ed., 1981.

[56] J. Parker and S. D'Angelo, "A digital model of the Buchla Lowpass Gate," in *Proc. Int. Conf. Digital Audio Effects (DAFx-13)*, Maynooth, Ireland, Sept. 2–5 2013.

[57] K. J. Werner and J. O. Smith III, "An energetic interpretation of nonlinear wave digital filter lookup table error," in *Proc. IEEE Int. Symp. Signals, Circuits, Syst. (ISSCS)*, Iaşi, Romania, July 9–10 2015.

[58] R. M. Corless, G. H. Gonnet, D. E. G. Hare, D. J. Jeffrey, and D. E. Knuth, "On the Lambert W function," *Adv. Computational Math.*, vol. 5, no. 1, pp. 329–359, 1996.

[59] T. P. Dence, "A brief look into the Lambert W function," *Appl. Math.*, vol. 4, pp. 887–892, June 2013.

[60] Electrosmash, "Tube Screamer analysis," `http://www.electrosmash.com/tube-screamer-analysis`.

[61] R. G. Keen, "The technology of the Tube Screamer," 1998, `http://www.geofex.com/article_folders/tstech/tsxtech.htm`.

[62] A. Vladimirescu, *The SPICE Book*, John Wiley & Sons, New York, 1994.

[63] R. Donley, "QR-decomposition for a 2×2 matrix," `https://youtu.be/51MRHjKSbtk`, June 14 2011.